Nanowire architectures improve ion uptake kinetics in conjugated polymer electrochemical transistors

Rajiv Giridharagopal, ¹ Jiajie Guo, ² Jessica Kong, ¹ David S. Ginger^{1*}

¹Department of Chemistry, University of Washington, Seattle, Washington, USA 98195

²Molecular Engineering and Sciences Institute, University of Washington, Seattle, Washington, USA

98195

*Corresponding author: dginger@uw.edu

ABSTRACT

Organic electrochemical transistors are believed to face an inherent materials design tension

between optimizing for ion mobility and for electronic mobility. These devices transduce ion uptake into

electrical current, thereby requiring high ion mobility for efficient electrochemical doping and rapid turn-

on kinetics, and high electronic mobility for maximum transconductance. Here we explore a facile route to

improve operational kinetics and volumetric capacitance in a high mobility conjugated polymer (poly[2,5-

(2-octyldodecyl)-3,6-diketopyrrolopyrrole-alt-5,5-(2,5-di(thien-2-yl)thieno [3,2-b]thiophene)], DPP-DTT)

by employing a nanowire morphology. For equivalent thicknesses, the DPP-DTT nanowire films exhibit

consistently faster kinetics (~6-10X faster) compared to a neat DPP-DTT film. The nanowire architectures

show higher volumetric capacitance, consistent with the porous structure enabling faster, less inhibited ion

uptake throughout the film. The nanowires also exhibit a small but energetically favorable shift in the

threshold voltage, making the nanostructured system both faster and energetically easier to

electrochemically dope compared to neat films. We explain the variation using two atomic force

microscopy methods: in situ electrochemical strain microscopy (ESM) and nanoinfrared imaging via

photoinduced force microscopy (PiFM). These data indicate that the nanowire film's structure allows

1

greater swelling and ion uptake throughout the active layer, indicating that the nanowire architecture exhibits volumetric operation whereas the neat film is largely operating via field-effect. We propose that, for higher-mobility materials, casting the active layer in nanowire form may offer faster kinetics, enhanced volumetric capacitance, and possibly lower threshold voltage while maintaining desirable device performance.

INTRODUCTION

Conjugated polymers have seen increasing use in mixed electronic-ionic devices in recent years, 1,2 from polymeric supercapacitors, 3,4 to neuromorphic computing architectures, $^{5-7}$ to organic electrochemical transistors (OECTs) for biosensing, $^{8-14}$ The push for better devices has spurred rapid advances in understanding the basic materials properties in these organic mixed ionic-electronic conductors that influence OECT operation. OECTs operate by transducing ion uptake into electrical conductivity, where the source of ions is typically an aqueous electrolyte serving as the gate dielectric. The application of a gate bias (V_G) to the electrolyte induces ion motion into (or out of) the semiconductor to compensate for an injected electronic charge, resulting in electrochemical doping of the active layer and an increase in the source-drain current, I_{DS} . Understanding the mechanisms underlying this ion uptake process is critical for enabling rational design of OECT materials. For example, polymeric semiconductors exhibit variations in ion uptake due to crystallinity, 17,18 the anion species, 14,19 sidechain functionalization, $^{18,20-22}$ and water uptake from aqueous electrolytes. 14,23,24

OECTs offer the benefit of volumetric capacitance, wherein the three-dimensional active layer accommodates ions and therefore dramatically increases the capacitance,²⁵ as opposed to purely field-effect operation near the electrolyte-semiconductor interface as in electrolyte-gated field effect transistors (EG-OFETs). The commonly used metric of performance when evaluating an OECT is the product of carrier mobility (μ) and the volumetric capacitance (C^*),²⁶ μC^* . The transconductance (dI_{DS}/dV_G , or g_m) and μC^*

are linked through the conventional field-effect transistor equation, which, in the saturation regime, is given by:

$$\frac{\Delta I_{DS}}{\Delta V_G} = g_m = \mu C^* \frac{Wd}{L} (V_T - V_G) \tag{1}$$

Here, I_{DS} is source-drain current, μ is the carrier mobility (cm²/V-s), C^* is the volumetric capacitance (F/cm 3), W is the channel width, L is the channel length between source and drain electrodes, d is the film thickness, V_T is the threshold voltage, and V_G is the gate voltage. From this equation, the key materialsrelated factor in enabling high g_m is μC^* , where μ largely depends on the order in the polymer and C^* depends upon the ability to store charge throughout the film via ion injection. Although not captured directly by the μC^* product, we emphasize here that turn on kinetics are also an important design consideration although a large C^* is desirable, if the turn on/turn off kinetics are too slow the material will remain impractical for many applications. Thus, an ideal OECT material architecture would allow efficient ion injection throughout the film (high C^* , rapidly achieved) while conducting electronic charge through a highly ordered subset of active sites (high μ).²⁷ In organic field effect transistors (OFETs), many groups have reported that polymer nanowires can enable enhanced mobility, 27-30 and for electrochemical applications, these structures could enable efficient volumetric doping due to the geometrical advantages of high-surface area nanowire geometries. Indeed, many approaches to improve OECT performance, from acid treatment^{31,32} and ionic liquid-based enhancement³³ of PEDOT:PSS, to freeze-drying/lyophilization^{34,35} may already result in nanotexturing of the conjugated polymer semiconductor. Herein, we explicitly consider nanowire architectures.

For high- μ materials, diketopyrrolopyrrole polymers have been reported in a few electrochemical devices. ^{36,37} As field-effect transistor materials, these polymers exhibit some of the highest reported hole mobilities of semiconducting polymers, on the order of $10 \text{ cm}^2/\text{V-s}$, ^{38–40} thereby enabling high g_m values while also offering potential advantages in ambipolar transport for more complex device topologies. ⁴⁰ Recent reports have shown that the donor-acceptor polymer poly[2,5-(2-octyldodecyl)-3,6-diketopyrrolopyrrole-alt-5,5-(2,5-di(thien-2-yl)thieno [3,2-b]thiophene)] (DPP-DTT) (**Fig. 1A**) can be

made into nanowire structures by mixing with polystyrene (PS) in a common solvent and exploiting the different relative solubility of the components to remove the PS,⁴¹ similar to work done in other DPP-based polymers⁴² and more broadly in the OFET community.³⁷

Given the advantages of high hole mobility, straightforward nanowire formation, and existing interest in DPP-based polymers for aqueous electrolyte devices, DPP-DTT is a natural platform to test the hypothesis that nanowire morphologies could improve OECT operation. Here, we report the use of DPP-DTT in OECTs and demonstrate that nanowires consistently enable 6-10X faster ion uptake compared to the standard DPP-DTT film, while maintaining similar μC^* . We show consistently lower threshold voltages for nanowire films and that nanowires enable higher C* values. Finally, we use electrochemical strain microscopy and photoinduced force microscopy to verify that the nanowires are accommodating ions directly throughout the bulk of the film, rather than merely enabling more efficient field-effect functionality or simply being higher mobility, thereby showing that nanowires enable enhanced volumetric capacitance compared the field-effect operation of unstructured DPP-DTT.³⁸ We find that the mobilities when doped are similar³⁸ and the device benefit is primarily capacitance. While the hydrophobic nature and highest occupied molecular orbital (HOMO) level of -5.2 eV³⁹ preclude DPP-DTT specifically from becoming a champion OECT material, this method of enabling faster kinetics with the same device performance is a useful platform for maximizing OECT functionality in a given system, for example in emerging glycolated DPP-derivatives. 14,43-45 Such a method is useful in the context of enabling rational design of faster or more sensitive OECT-based biosensors.⁴⁶

RESULTS AND DISCUSSION

We formed DPP-DTT nanowires by blending DPP-DTT and polystyrene (PS) in a common solvent with varying ratios. The different solubilities result in segregation and ultimately formation of DPP-DTT nanowires in solution.³⁹ Hereafter, we refer to these samples in terms of DPP-DTT:PS ratio in solution. A 2:8 ratio means 1 mL of 20 mg/mL DPP-DTT was added to 4 mL of 20 mg/mL PS (see Experimental Methods). A 1:0 ratio means a neat DPP-DTT solution (no PS). For the blended films, the PS is then

removed from the cast films by submerging them in toluene for ~3-5 minutes; this process can be verified by imaging the same area before and after washing using AFM (**Fig. S1**) and by spectroelectrochemistry (**Fig. S11**). For the films here, unless mentioned otherwise, the concentration of DPP-DTT in the combined solution was kept at 4 mg/mL. This process yields films of thickness ~35-55 nm based on AFM measurements, with higher values for neat films and lower for 2:8 nanowires, but very different structure (**Fig. 1B-D**). The 2:8 nanowires are easily observed (**Fig. 1C**), while 4:6 are evident but less anisotropic (**Fig. 1D**). The topography for neat films (**Fig. 1B**) is similar to that reported in other work.⁴⁰

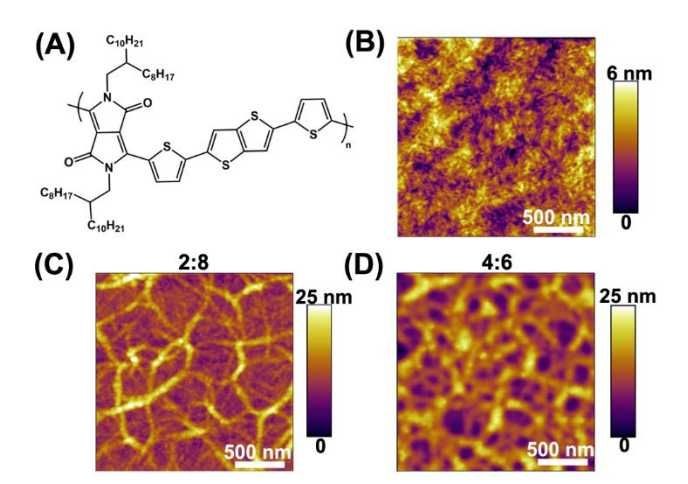


Figure 1. DPP-DTT films of different nanowire geometries. (A) Chemical structure of DPP-DTT (B) DPP-DTT neat film (not nanowires), ~45-50 nm thick. (C) DPP-DTT nanowires formed using a 2:8 DPP-DTT:polystyrene solution, then removing the polystyrene using toluene, ~35-40 nm thick. (D) Nanowires using a 4:6 ratio, ~40-45 nm thick.

Device Measurements:

We first show that the nanowire films form functional OECTs through conventional device measurements. In these devices, we use a Ag/AgCl electrode as a gate electrode, and we used 100 mM potassium hexafluorophosphate (KPF₆) as the electrolyte. For these devices, V_T is typically around -0.5 V in KPF₆; using Cl⁻ as the anion pushes the V_T to nearly -0.75 V as seen in other reports,⁴¹ resulting in many

cases where the g_m value does not reach a peak within the electrochemical water window. Given that the focus on our study is the nanowire geometry and not the anion-dependence, we use 100 mM KPF₆ to ensure g_m values reach a peak that can be compared across geometries.

DPP-DTT Ratio	$V_{T}(V)$	μC*(F cm ⁻¹ V ⁻¹ s ⁻¹)	C* (F cm ⁻³)	μ_{OECT} (cm ² V ⁻¹ s ⁻¹) (saturation)	$\mu \text{ (cm}^2 \text{ V}^{-1} \text{ s}^{-1})$ (calculated from μC^*)
1:0	-0.519±0.02	123.4	7.1 ±0.6	7.28±1.3	16.0
4:6	-0.509±0.03	107.2	8.7±0.9	7.38±1.1	12.4
2:8	-0.502±0.01	132.3	27.7±1.1	7.16±1.0	5.6

Table 1. OECT Performance of DPP-DTT Devices.

Fig. 2A shows typical transfer and g_m curves for DPP-DTT devices, with representative output curves in Fig. S5. Here, the threshold voltage is slightly more negative (~17 mV) for 1:0 than for 4:6 and 2:8 films, indicating that it is energetically easier for anions to dope the nanowire films and enable conduction regardless of W/L (Fig. S2). In Fig. S2 we show the normalized g_m value average over many devices (~35-40 devices tested per ratio). This threshold shift occurs at very slow sweep rates (20 s per 0.025 V step, see Methods), with no observable hysteresis between forward and reverse sweeps at these rates, indicating that it is a physical effect and not from experimental artifact. This effect is similar to the V_T shift observed in DPP-DTT nanowire OFETs.⁴⁴

We show aggregated device data for the three different dimensions in **Fig. 2B** and **Table 1**. These data are aggregated by varying the electrode geometry (see Experimental section), and error bars represent the standard deviation of the mean for devices of the same W/L dimensions. The devices exhibit similar g_m , and using equation (1), we can extract an approximate μC^* from these data. The μC^* data indicate that these all operate with similar performance on the order of ~100 F/cm·V·s. Notably, these devices are similar despite the 1:0 film being ~10 nm (~15%) thicker on average than a 2:8 nanowire device films. As g_m is well-known to scale with active layer thickness due to volumetric capacitance,⁴⁷ if the active layer thickness was the sole cause of the differences between these films then the 2:8 nanowires would perform

significantly worse than the neat films. Variations in the largest devices (W/L = 200) are attributed to increases in contact resistance (or other parasitic resistance) from ion concentration at the drain due to larger geometry.⁴⁸

By comparing the data to electrochemical impedance spectroscopy (EIS), we observe an improvement in the volumetric capacitance (C^*). The 1:0, 4:6, and 2:8 films show volumetric capacitance values of ~8, 9, and 28 F/cm³, respectively (**Fig. S12, S13**). By measuring the mobility via saturation current, we extract hole mobilities on the order of ~7 cm²/V-s, with the 2:8 films having similar if slightly *lower* mobility if instead calculating via μC^* and EIS (**Table 1**). While at first surprising, the complex structure-function relationship in aqueous gating has a significant effect on the electronic behavior. For example, it has been shown that increasing the dry mobility can decrease the OECT mobility due to the effect of hydration on the polymer structure.⁴⁶ We discuss the competing effects of swelling and crystalline structure on kinetics and volumetric capacitance below.

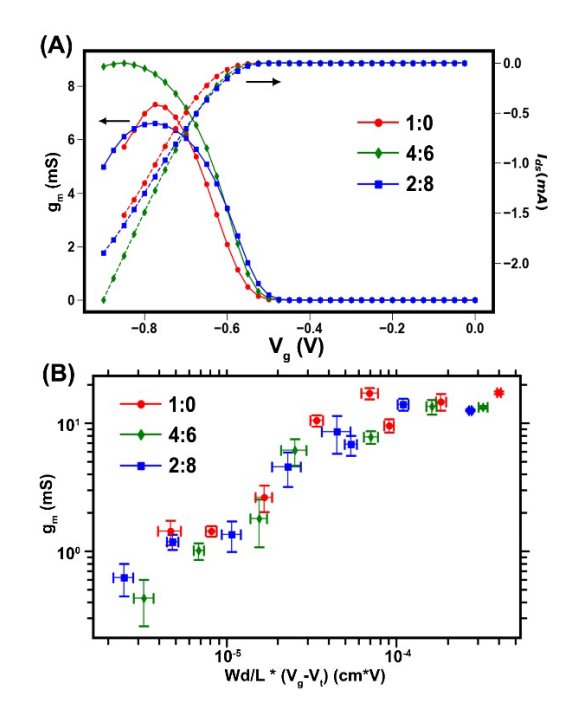


Figure 2. DPP-DTT OECT device data. (A) Typical transfer curve and transconductance for 1:0, 4:6, and 2:8 films in 100 mM KPF₆, plotted versus gate-source voltage V_G . (B) g_m statistics plotted against the DPP-

DTT structure. Here, the data are averaged for devices of the same W/L ratio with film thickness held approximately constant, and error bars represent standard deviation of the mean g_m value and the (V_G-V_T) value, where V_G is the gate voltage for peak g_m .

The nanowire architecture favorably shifts the threshold voltage while maintaining similar current-transport properties to a conventional film. This threshold voltage shift could occur because the nanowires shift the HOMO level to enable easier oxidation, as is common with more ordered conjugated polymer films, 49 or the nanowires could enable better accessibility to the three-dimensional volume of the film. While g_m scales with film thickness, 47 device data are acquired at steady-state conditions and cannot discriminate between these possibilities alone. Device kinetics indicate that the 2:8 nanowire case exhibits faster I_{DS} (18% up to 47%) in response to a gate voltage compared to the neat film (**Fig. S3**) with reasonably similar cycling stability (**Fig. S4**). For the remainder of this work, we focus on the two extreme cases (2:8 and 1:0) to better examine how nanostructuring can improve operation. Although EIS can also be used to extract characteristic time constants, 50 we primarily use time-dependent measurements for direct comparison.

Spectroelectrochemistry:

We next use spectroelectrochemistry to investigate the kinetics and the mechanism involved in ion uptake. To better focus on the difference between DPP-DTT nanowire networks and neat films in the context of electrochemical transistors, we turn our attention primarily to comparing 2:8 and 1:0 films. In **Fig. 3A-B**, we compare the spectra taken in KPF₆ at different voltages over 20 seconds. For the nanowires, we see clear evidence of vibronic peaks associated with the highly crystalline structures,⁵¹ with a 0-0 vibrational peak at ~820 nm red-shifted relative to the peak absorption in the neat film at ~800 nm, similar to that reported for DPP-DTT nanowires in dry conditions.⁴⁹ These spectra indicate that the 2:8 film is more highly ordered. Zhang et al. showed that DPP-DTT films are crystalline in the bulk but disordered at the liquid interface;⁵² our results with thicker DPP-DTT films (**Fig. S6**) match this interpretation, with ~130

nm films showing these vibronic spectra due to higher percentage of the film being inaccessible to the water layer. We propose that the nanowires seem to retain higher level of crystallinity at the liquid interface compared to the neat films.

Upon application of a gate voltage just beyond V_T (Fig. 3A, B, where V_G = -0.6 V), the spectra for the nanowires exhibit a clear reduction of the main absorbance peak centered ~800 nm and an associated increase in polaron absorption >900 nm. For the film, this process over the same period is much slower. At higher bias far beyond threshold (Fig. 3C, D, where V_G = -1 V), the process is faster in both neat films and nanowire films. An initial assumption might be that the kinetics are faster due only to the favorable shift in threshold voltage. To rule out this effect, we plot the kinetics at 800 nm across a range of bias voltages in Fig. 4A. Here, the time constants show a clear difference between the two geometries. Fig. 4A plots the time constant based on a single exponential fit to the kinetics for a range of $V_G > V_T$ (when the device is turned on). At just beyond threshold, the nanowires are ~6X faster, and at -1 V (saturation) they are ~10X faster. As suspected from the V_T shift in the device data, the nanowires are indeed easier to electrochemically dope than the unstructured film. The threshold can be estimated from the absorbance data (Fig. S6B, Fig. S7) as well as cyclic voltammetry (Fig. S14), showing the same threshold voltage shift between nanowires and films. This difference in kinetics holds across wavelengths at each voltage (Fig. 4B, Fig. S10), indicating that the kinetics variation is more than just threshold voltage shift between the film and nanowire. Here the plots show the rate $(1/\tau, \tau)$ is the single exponential time constant) for sake of clarity. Switching from KPF₆ to NaCl significantly slows down the kinetics (Fig. S8), but the comparative behavior of nanowires versus films remains the same (i.e. nanowire films still show ~ 1.5 -2X faster kinetics). While μC^* could be impacted by thickness because of the increased accessibility of polymer or diffusion-limited transport,53 the kinetics trends across various thicknesses seems to rule that out as the sole contributing factor (Fig. 4C).

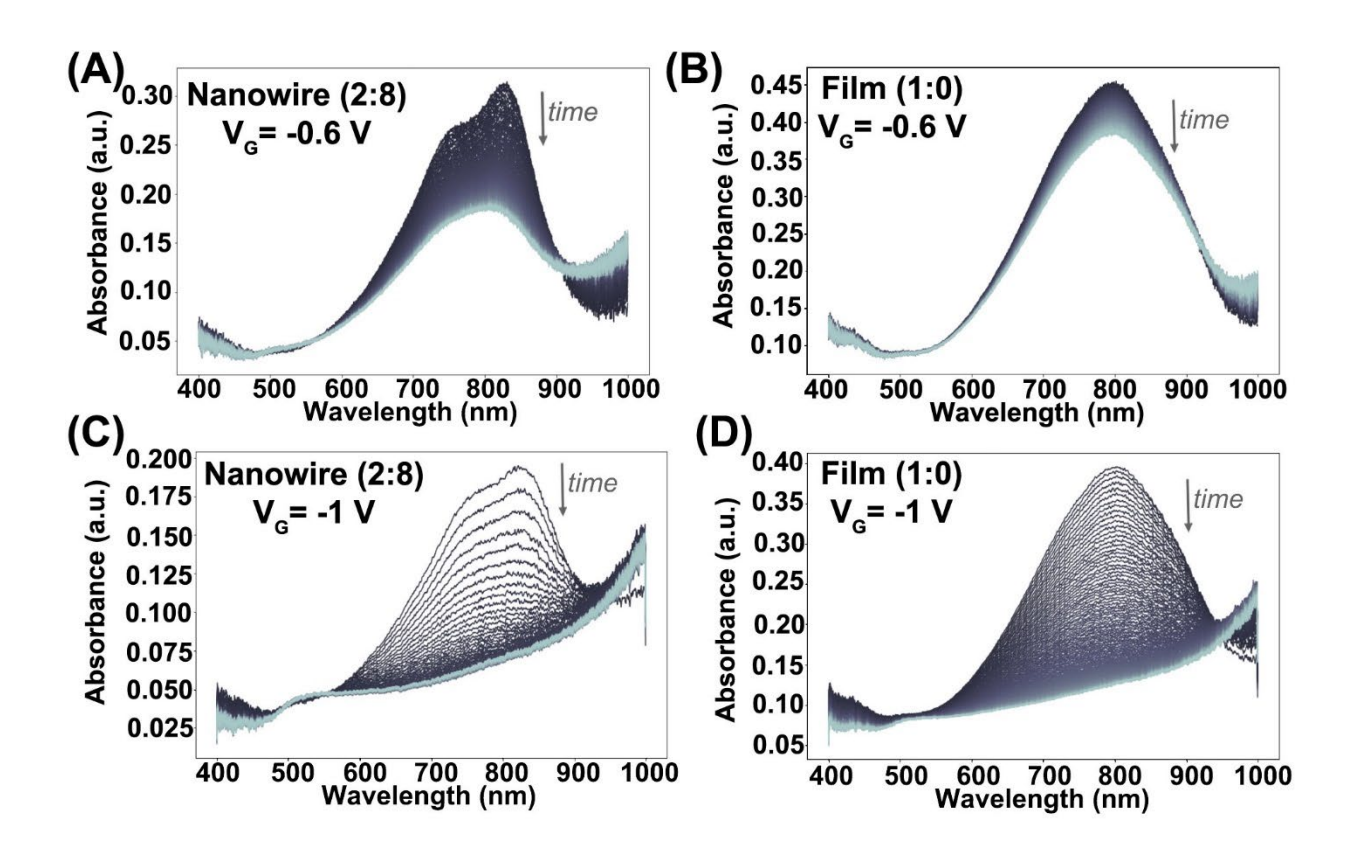


Figure 3. Spectroelectrochemistry of DPP-DTT nanowires versus films. (A) Absorbance spectra with the gate (Ag/AgCl) at -0.6 V, barely beyond V_T , for 2:8 nanowires and (B) 1:0 neat film. Spectra are acquired during the first 20 s after a gate bias is applied. (C) Absorbance spectra with the gate at -1 V for 2:8 nanowires and (D) 1:0 neat film. -1 V is far beyond V_T for these materials. These data show the significant kinetics benefit from nanowires at near threshold voltage conditions and in saturation conditions. These data were taken in 100 mM KPF₆.

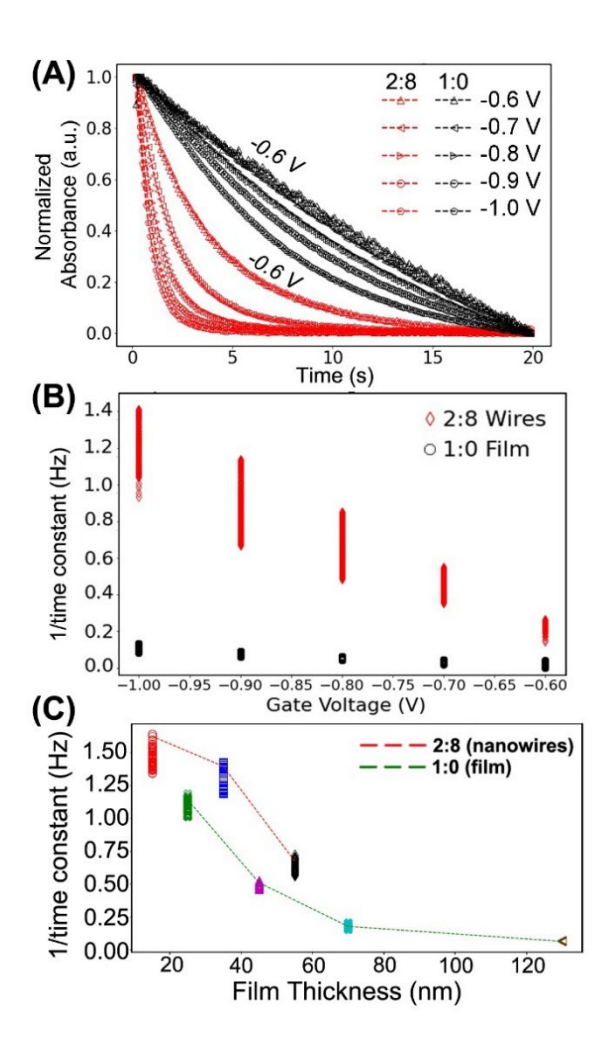


Figure 4. Kinetics of DPP-DTT nanowires. (A) Normalized absorbance versus time for 2:8 (nanowire) and 1:0 (neat) films from -0.6 V to -1.0 V at 800 nm, spanning conditions barely above threshold and far above threshold, respectively. The curve corresponding to -0.6 V for each ratio is labeled for clarity. (B) The rate constant $(1/\tau, \tau)$ is the single exponential time constant) as a function of gate voltage. The rate constant shown for each gate voltage is measured from spectroelectrochemistry at each wavelength from 600 to 900 nm. The nanowires are ~6-10X faster at each voltage. (C) The rate constant for various thicknesses for 2:8 and 1:0 films, plotted for each rate measured from 730 to 850 nm for each film. These data confirm that the improved kinetics are due to the structure and not just film thickness-- at a given overall thickness, the 2:8 devices are faster.

The nanowire geometry therefore seems to permit oxidation of the film both at lower threshold voltage and faster than in the neat film. These data seem to indicate that the nanowires are not necessarily benefiting from enhanced mobility but rather from a morphological effect wherein the volume of the film is more easily accessible by injected ions. Indeed, studies of poly(3-hexylthiophene) have shown that absorbance kinetics in thin active layers are limited more by ion injection than diffusion within the active layer, 53,54 and we interpret these data as consistent with that interpretation.

Scanning Probe Analysis:

Taking these data into account, we turn to scanning probe methods to provide a real-space answer for two remaining questions. First, why does changing the morphology of the film result in an improvement in kinetics? Secondly, why do the nanowires show higher C^* but lower μ ? To answer these questions, we first probe the nanoscale structure using electrochemical strain microscopy (ESM), ^{18,52} which probes the swelling of the polymer *in situ* due to ion injection into the film. In **Fig. 5**, we use ESM as a function of tip-bias for a neat film and a nanowire film. In **Fig. 5B**, we observe swelling all over the film, with slightly higher swelling in areas between the top-most nanowires. The AFM cantilever in this case acts as the gate, so in **Fig. 5C** we plot the ESM amplitude as a function of tip voltage for a 2:8 and a 1:0 film. We observe a significant increase in the swelling on the nanowire film beyond threshold voltage conditions (at negative tip voltages) compared to the neat film, which is consistent with enhanced ion injection for the nanowire case.

Finally, we use photoinduced force microscopy (PiFM) on films that have been doped *ex situ* and imaged with PF₆⁻ remaining, as we have done in previous work. ^{18,55} PiFM is an nanoinfrared AFM method that allows mapping of vibrational spectra with high spatial resolution. The spectra of the nanowires are shown in **Fig. S15**. While the topography in the 2:8 nanowires does not show any obvious structure, the PiFM data reveal very strong presence of PF₆⁻ (\sim 840 cm⁻¹) with evidence of PiFM signal in areas between the topmost wires consistent with uptake into the film (**Fig. 6, Fig. S17**). By comparing the data taken on neat films and nanowires at the doping interface, the neat 1:0 films exhibit significant topographic changes

at the surface consistent with less ion diffusion into the bulk (**Fig. S17C**, **Fig. S18**). The aggregation of ions near the 1:0 film surface is consistent with previous reports of largely electrolyte-gated field effect operation as opposed to volumetric operation.⁵² These AFM data therefore show that the nanowire benefits relative to the neat film arise primarily from morphology, with the high surface area and nanowire structure better enabling ion uptake. This observation agrees with liquid interfacial studies showing that a disordered ~2 nm layer in DPP-DTT can determine charge transport properties;⁵² here, the nanowires are a porous network, and effectively the volume of the film is perhaps within the liquid interface given the difference in ESM amplitude.

These scanning probe data also yield a potential hypothesis to address the second question regarding the mobility. As has been shown in previous work, 18 ion uptake and associated water molecules can have surprising effects on the performance by disrupting crystallinity. We hypothesize that because the nanowire films swell more than the neat film during operation, this swelling disrupts the crystallinity of the DPP-DTT nanowire network and lowers the mobility. As a result, despite being able to more easily accommodate ions volumetrically (showing higher C^*), the nanowires may also show lower mobility.

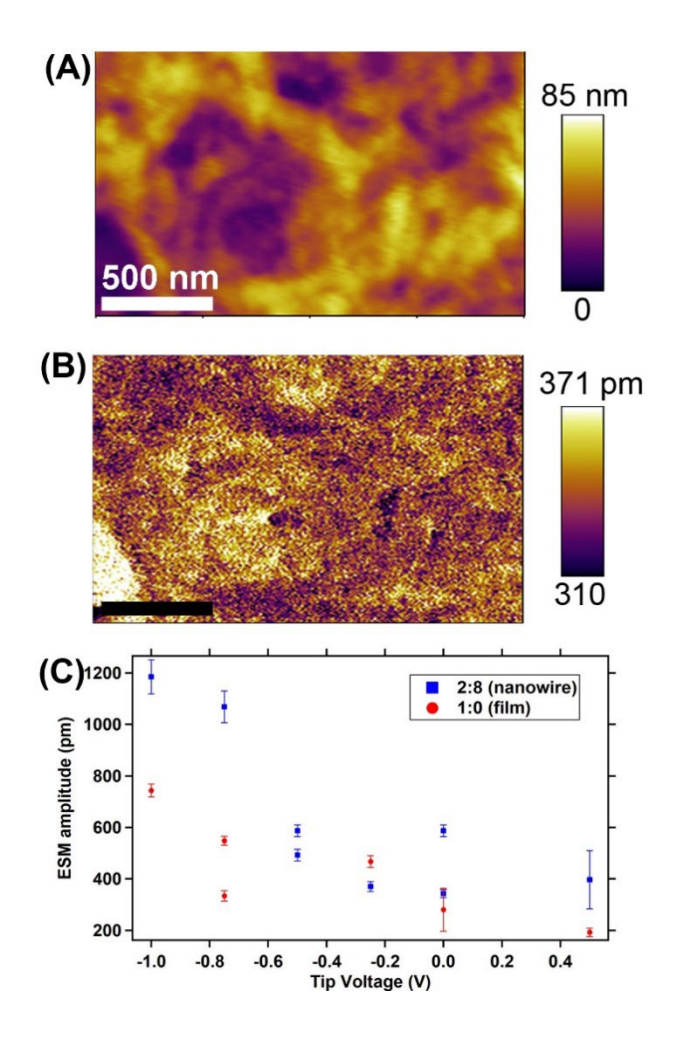


Figure 5. ESM Amplitude versus Geometry. (A) Topography and (B) ESM amplitude of a 2:8 (nanowire) film in 20 mM KPF₆. Here the ESM amplitude is taken with V_{AC} =500 mV (i.e. centered at 0 V +/- 250 mV) and V_{tip} = 0 V. (C) ESM amplitudes for a 2:8 and 1:0 layer across a range of V_{tip} values, with the error bars representing standard deviation in the amplitude response. The 2:8 nanowire device shows higher amplitudes than the 1:0 conventional DPP-DTT film, particularly when the V_{tip} is past the threshold for consistent doping at -0.5 V. These data are consistent with the hypothesis that the nanowires exhibit enhanced ion uptake due to their geometry relative to the non-nanowire film.

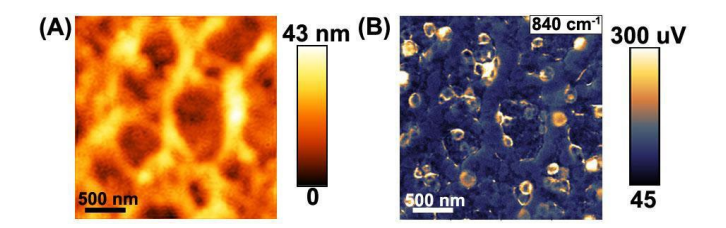


Figure 6. Photoinduced Force Microscopy (PiFM) of PF₆⁻ Dopants in DPP-DTT Nanowires. (A) Topography and (B) PiFM at 840 cm⁻¹ of a 2:8 DPP-DTT nanowire film, corresponding to the PF₆⁻. The film was electrochemically doped using 100 mM KPF₆ and a Ag/AgCl gate at $V_G = -0.85$ V for ~60 s.

CONCLUSIONS

We have shown that in a high-mobility polymer, DPP-DTT, we can improve the kinetics by employing nanowire structures instead of a conventional neat film. We demonstrate that, while optimizing for mobility is important in OECTs, it is important to consider that C^* (volumetric capacitance) is linked to how easily ions can diffuse into the three-dimensional volume. The nanowire structures exhibit faster kinetics at all voltages, and a slightly lower threshold voltage, which we attribute to the nanowires allowing lower structural barrier for ion diffusion into the film. The nanowires also exhibit higher C^* . We verify this result through real-space imaging in various correlated AFM modalities, showing that the nanowires indeed swell under bias and that the DPP-DTT system exhibits volumetric response as an OECT rather than through a field-effect. Although the hydrophobic nature and comparatively large threshold voltage preclude DPP-DTT from practical OECT device applications, and the limited operational window due to the HOMO level narrows the potential biologically-relevant application range, the data here present a platform for simple optimization on state-of-the-art materials that are under development.

ACKNOWLEDGMENTS

This paper is based primarily on preliminary work begun under National Science Foundation grant DMR-1607242 and completed under DMR-2003456. We acknowledge additional support for data science

methods development to analyze the PiFM data (J.K.) from NSF EAGER DMR-1842708. J.K. also received student fellowship support from the Clean Energy Institute and National Science Foundation Research Traineeship under award NSF DGE-1633216. We thank Lucas Q. Flagg and Connor G. Bischak for helpful discussions. Part of this work was conducted at the Molecular Analysis Facility, a National Nanotechnology Coordinated Infrastructure site at the University of Washington which is supported in part by the National Science Foundation (grant NNCI-1542101), the University of Washington, the Molecular Engineering & Sciences Institute, the Clean Energy Institute, and the National Institutes of Health.

EXPERIMENTAL

Film formation:

Poly[2,5-(2-octyldodecyl)-3,6-diketopyrrolopyrrole-alt-5,5-(2,5-di(thien-2-yl)thieno[3,2-b]thiophene)] (DPP-DTT, Ossila) and polystyrene (PS, Sigma-Aldrich) were dissolved separately in dichlorobenzene in a nitrogen glove box. These solutions were stirred at no higher than 60 °C and 600 RPM for at least 2 hours. For the ratios specified in the paper (2:8 and 4:6), the solutions were mixed based on volume ratio. The desired target was 4 mg/mL DPP-DTT per mL of mixed solution. To achieve this, for 2:8 films we make separate solutions of DPP-DTT and PS at 20 mg/mL, and for 4:6 films we make separate solutions at 10 mg/mL. For neat DPP-DTT (i.e. a ratio of 1:0 DPP-DTT:PS), we dissolve at 4 mg/mL. All mixed solutions were stirred at 60 °C and 600 RPM overnight. We spincoat the solution on plasma-cleaned substrates using 3 s at 500 RPM, 150 s at 1500 RPM, then 10 s at 2000 RPM. Typically, the solutions are heated at approximately 30 °C prior to spincoating. The films are annealed at 200 °C under flowing nitrogen for 5 minutes. For removing PS, we submerge the films in toluene for at least 5 minutes. The films are then stored in vacuum.

Device measurements:

For device measurements, we use custom-fabricated gold electrodes on polyethylene terephthalate substrates (Nano Terra) or evaporated on glass. The electrodes are all with 20 µm channel lengths and

channel widths of 4000, 2000, 1000, 800, 400, 200, and 100 µm. Devices are prepared in a similar manner to films using the procedure above, though for most devices we anneal at 180 °C to avoid warping the polyethylene terephthalate substrate; annealing at either 180 °C or 200 °C had no discernible effect on device performance. Prior to measuring the device performance we remove excess polymer under a microscope using acetone to wet an absorbent swab similar to that in our previous work, ^{13,18} then we cover all of the device except the active area and the contact electrodes to the source/drain with clear nail polish (Sally Hansen Insta-Dri Top Coat). Optical images and device data show no damage to the active layer; an example of the substrate is shown in Figure S19. The electrolyte used was typically 100 mM KPF₆ or 100 mM KCl, with both degassed with nitrogen for ~10 minutes prior to use. The gate electrode is a standard Ag/AgCl electrode. The device measurements are acquired using LabView code that operates two Keithley 2400 source-measure units. This code, along with a Python version, is publicly available upon request. All devices are cycled once prior to measurement, and all the device data shown use both the trace and retrace. Typical measurement times are 20 s per point in the transfer curves (or 800 s/V), with 120 s wait time prior to the first data point to ensure steady-state doping conditions are reached. Analysis was performed using custom Python code; this code is publicly available (https://github.com/GingerLabUW/oect processing). The threshold voltages are calculated using linear fits to $I_{DS}^{1/2}$ vs V_G plots. Transconductance (g_m) was calculated using a derivative of the transfer curve directly.

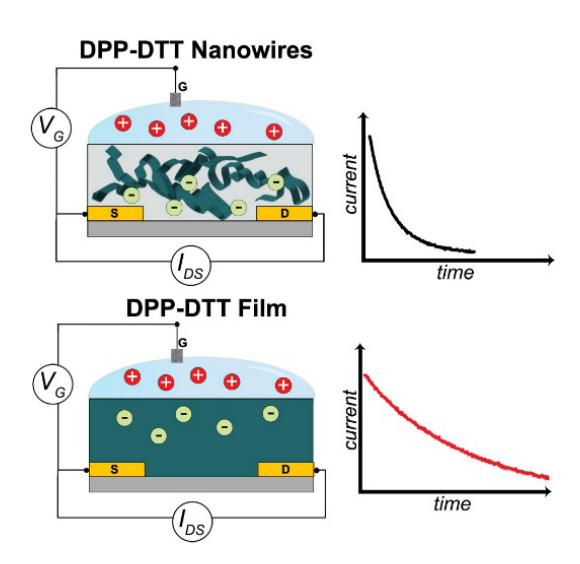
Spectroelectrochemistry and Electrochemical Impedance:

For spectroelectrochemistry, we use a MetroOhm PGSTAT204 to operate our device and an Agilent 8453 spectrometer for recording the data. For these measurements we spincoat the film on FTO substrates (Sigma Aldrich). We use a Ag/AgCl as the reference electrode and a Pt mesh as the counter electrode. We cycle each device with a C-V curve three times prior to measurement. The data are analyzed in Python via the above publicly available code. For electrochemical impedance, we use the devices with pre-fabricated electrodes where two $600 \times 600 \,\mu\text{m}^2$ Au patches are used as the substrate. The devices are cycled from -0.9 V to $0.9 \,\text{V}$ at $0.05 \,\text{V/s}$ and analyzed via the MetroOhm NOVA software.

Scanning Probe Microscopy:

AFM measurements were performed on two instruments. The ESM experiments were performed on an Asylum Research Cypher-ES system, as were AM-FM/stiffness measurements. The topography, including scratch edge images for film thickness measurements, and other AFM data were acquired on an MFP-3D. For the ESM data, we use 20 mM KPF₆ as the electrolyte during measurement; for other AFM measurements, the samples are in a closed cell under flowing nitrogen. For photoinduced force microscopy (PiFM), we used a Molecular Vista VistaScan system with a Block Laser quantum cascade laser capable of infrared excitation from 760 cm⁻¹ to 1850 cm⁻¹. For AM-FM we typically use Budget Sensors ElectriMulti75-G tips (~2 N/m, ~75 kHz). For PiFM, we use Mikro-Masch HQ:NSC15 tips (~30 N/m, ~325 kHz). For ESM we use Budget Sensors ContGB tips (~0.2 N/m, ~13 kHz); in ESM, the amplitude can increase by using lower stiffness cantilevers, so users are cautioned to avoid comparing data taken with very different tips. We use the second resonance mode for topography and the first mode for imaging. For the doping experiments, we bias the film relative to a AgCl substrate in 100 mM KPF₆, then quickly rinse in DI water and dry under nitrogen. The films will show a noticeable color change due to doping; for DPP-DTT, the films become visually clear because of the polaron feature stretching past the visible range.

TABLE OF CONTENTS GRAPHIC



SUPPORTING INFORMATION

Additional topography data pre-/post-PS removal, device data, additional spectroelectrochemistry in KPF₆ and NaCl data, electrochemical impedance, PiFM spectra and images of DPP-DTT and PS.

REFERENCES

- (1) Paulsen, B. D.; Tybrandt, K.; Stavrinidou, E.; Rivnay, J. Organic Mixed Ionic-Electronic Conductors. *Nat. Mater.* **2020**, *19* (1), 13–26. https://doi.org/10.1038/s41563-019-0435-z.
- (2) Ohayon, D.; Inal, S. Organic Bioelectronics: From Functional Materials to Next-Generation Devices and Power Sources. *Adv. Mater.* **2020**, e2001439. https://doi.org/10.1002/adma.202001439.
- (3) Meng, Q.; Cai, K.; Chen, Y.; Chen, L. Research Progress on Conducting Polymer Based Supercapacitor Electrode Materials. *Nano Energy* 2017, 36, 268–285. https://doi.org/10.1016/j.nanoen.2017.04.040.
- (4) Zhao, Z.; Richardson, G. F.; Meng, Q.; Zhu, S.; Kuan, H.-C.; Ma, J. PEDOT-Based Composites as Electrode Materials for Supercapacitors. *Nanotechnology* 2016, 27 (4), 042001. https://doi.org/10.1088/0957-4484/27/4/042001.
- (5) van de Burgt, Y.; Lubberman, E.; Fuller, E. J.; Keene, S. T.; Faria, G. C.; Agarwal, S.; Marinella, M. J.; Alec Talin, A.; Salleo, A. A Non-Volatile Organic Electrochemical Device as a Low-Voltage Artificial Synapse for Neuromorphic Computing. *Nat. Mater.* 2017, 16 (4), 414–418. https://doi.org/10.1038/nmat4856.
- (6) Keene, S. T.; Melianas, A.; Fuller, E. J.; van de Burgt, Y.; Alec Talin, A.; Salleo, A. Optimized Pulsed Write Schemes Improve Linearity and Write Speed for Low-Power Organic Neuromorphic Devices. J. Phys. D Appl. Phys. 2018, 51 (22), 224002. https://doi.org/10.1088/1361-6463/aabe70.
- (7) Keene, S. T.; Lubrano, C.; Kazemzadeh, S.; Melianas, A.; Tuchman, Y.; Polino, G.; Scognamiglio, P.; Cinà, L.; Salleo, A.; van de Burgt, Y.; Santoro, F. A Biohybrid Synapse with Neurotransmitter-Mediated Plasticity. *Nat. Mater.* 2020. https://doi.org/10.1038/s41563-020-0703-y.

- (8) Rivnay, J.; Wang, H.; Fenno, L.; Deisseroth, K.; Malliaras, G. G. Next-Generation Probes, Particles, and Proteins for Neural Interfacing. *Science Advances* 2017, 3 (6), e1601649. https://doi.org/10.1126/sciadv.1601649.
- (9) Faria, G. C.; Duong, D. T.; Salleo, A.; Polyzoidis, C. A.; Logothetidis, S.; Rivnay, J.; Owens, R.; Malliaras, G. G. Organic Electrochemical Transistors as Impedance Biosensors. MRS Communications 2014, 4 (4), 189–194. https://doi.org/10.1557/mrc.2014.35.
- (10) Rivnay, J.; Owens, R. M.; Malliaras, G. G. The Rise of Organic Bioelectronics. *Chem. Mater.* **2014**, 26 (1), 679–685. https://doi.org/10.1021/cm4022003.
- (11) Inal, S.; Rivnay, J.; Suiu, A.-O.; Malliaras, G. G.; McCulloch, I. Conjugated Polymers in Bioelectronics. Acc. Chem. Res. 2018, 51 (6), 1368–1376. https://doi.org/10.1021/acs.accounts.7b00624.
- (12) Rivnay, J.; Inal, S.; Salleo, A.; Owens, R. M.; Berggren, M.; Malliaras, G. G. Organic Electrochemical Transistors. *Nature Reviews Materials* 2018, 3, 17086. https://doi.org/10.1038/natrevmats.2017.86.
- (13) Bischak, C. G.; Flagg, L. Q.; Ginger, D. S. Ion Exchange Gels Allow Organic Electrochemical Transistor Operation with Hydrophobic Polymers in Aqueous Solution. *Adv. Mater.* 2020, 32 (32), e2002610. https://doi.org/10.1002/adma.202002610.
- (14) Flagg, L. Q.; Giridharagopal, R.; Guo, J.; Ginger, D. S. Anion-Dependent Doping and Charge Transport in Organic Electrochemical Transistors. *Chem. Mater.* 2018, 30 (15), 5380–5389. https://doi.org/10.1021/acs.chemmater.8b02220.
- (15) Flagg, L. Q.; Bischak, C. G.; Quezada, R. J.; Onorato, J. W.; Luscombe, C. K.; Ginger, D. S. P-Type Electrochemical Doping Can Occur by Cation Expulsion in a High-Performing Polymer for Organic Electrochemical Transistors. *ACS Materials Lett.* 2020, 254–260. https://doi.org/10.1021/acsmaterialslett.9b00501.
- (16) Friedlein, J. T.; McLeod, R. R.; Rivnay, J. Device Physics of Organic Electrochemical Transistors.

 Org. Electron. 2018, 63, 398–414. https://doi.org/10.1016/j.orgel.2018.09.010.

- (17) Giridharagopal, R.; Flagg, L. Q.; Harrison, J. S.; Ziffer, M. E.; Onorato, J.; Luscombe, C. K.; Ginger, D. S. Electrochemical Strain Microscopy Probes Morphology-Induced Variations in Ion Uptake and Performance in Organic Electrochemical Transistors. *Nat. Mater.* 2017, *16* (7), 737–742. https://doi.org/10.1038/nmat4918.
- (18) Flagg, L. Q.; Bischak, C. G.; Onorato, J. W.; Rashid, R. B.; Luscombe, C. K.; Ginger, D. S. Polymer Crystallinity Controls Water Uptake in Glycol Side-Chain Polymer Organic Electrochemical Transistors. J. Am. Chem. Soc. 2019, 141 (10), 4345–4354. https://doi.org/10.1021/jacs.8b12640.
- (19) Cendra, C.; Giovannitti, A.; Savva, A.; Venkatraman, V.; McCulloch, I.; Salleo, A.; Inal, S.; Rivnay, J. Role of the Anion on the Transport and Structure of Organic Mixed Conductors. *Adv. Funct. Mater.* 2018, 27, 1807034. https://doi.org/10.1002/adfm.201807034.
- (20) Giovannitti, A.; Sbircea, D.-T.; Inal, S.; Nielsen, C. B.; Bandiello, E.; Hanifi, D. A.; Sessolo, M.; Malliaras, G. G.; McCulloch, I.; Rivnay, J. Controlling the Mode of Operation of Organic Transistors through Side-Chain Engineering. *Proc. Natl. Acad. Sci. U. S. A.* 2016, *113* (43), 12017–12022. https://doi.org/10.1073/pnas.1608780113.
- (21) Giovannitti, A.; Maria, I. P.; Hanifi, D.; Donahue, M. J.; Bryant, D.; Barth, K. J.; Makdah, B. E.; Savva, A.; Moia, D.; Zetek, M.; Barnes, P. R. F.; Reid, O. G.; Inal, S.; Rumbles, G.; Malliaras, G. G.; Nelson, J.; Rivnay, J.; McCulloch, I. The Role of the Side Chain on the Performance of N-Type Conjugated Polymers in Aqueous Electrolytes. *Chem. Mater.* 2018, 30 (9), 2945–2953. https://doi.org/10.1021/acs.chemmater.8b00321.
- (22) Roncali, J.; Shi, L. H.; Garreau, R.; Garnier, F.; Lemaire, M. Tuning of the Aqueous Electroactivity of Substituted Poly(Thiophene)s by Ether Groups. *Synth. Met.* **1990**, *36* (2), 267–273. https://doi.org/10.1016/0379-6779(90)90060-X.
- (23) Savva, A.; Cendra, C.; Giugni, A.; Torre, B.; Surgailis, J.; Ohayon, D.; Giovannitti, A.; McCulloch, I.; Di Fabrizio, E.; Salleo, A.; Rivnay, J.; Inal, S. Influence of Water on the Performance of Organic Electrochemical Transistors. *Chem. Mater.* 2019, 31 (3), 927–937. https://doi.org/10.1021/acs.chemmater.8b04335.

- (24) Moser, M.; Hidalgo, T. C.; Surgailis, J.; Gladisch, J.; Ghosh, S.; Sheelamanthula, R.; Thiburce, Q.; Giovannitti, A.; Salleo, A.; Gasparini, N.; Wadsworth, A.; Zozoulenko, I.; Berggren, M.; Stavrinidou, E.; Inal, S.; McCulloch, I. Side Chain Redistribution as a Strategy to Boost Organic Electrochemical Transistor Performance and Stability. *Adv. Mater.* 2020, 32 (37), e2002748. https://doi.org/10.1002/adma.202002748.
- (25) Proctor, C. M.; Rivnay, J.; Malliaras, G. G. Understanding Volumetric Capacitance in Conducting Polymers. J. Polym. Sci. B Polym. Phys. 2016, 54 (15), 1433–1436. https://doi.org/10.1002/polb.24038.
- (26) Inal, S.; Malliaras, G. G.; Rivnay, J. Benchmarking Organic Mixed Conductors for Transistors. *Nat. Commun.* **2017**, *8* (1), 1767. https://doi.org/10.1038/s41467-017-01812-w.
- (27) Rivnay, J.; Inal, S.; Collins, B. A.; Sessolo, M.; Stavrinidou, E.; Strakosas, X.; Tassone, C.; Delongchamp, D. M.; Malliaras, G. G. Structural Control of Mixed Ionic and Electronic Transport in Conducting Polymers. *Nat. Commun.* 2016, 7, 11287. https://doi.org/10.1038/ncomms11287.
- (28) Tatum, W. K.; Luscombe, C. K. π-Conjugated Polymer Nanowires: Advances and Perspectives toward Effective Commercial Implementation. *Polym. J.* 2018, 50 (8), 659–669. https://doi.org/10.1038/s41428-018-0062-6.
- (29) Briseno, A. L.; Mannsfeld, S. C. B.; Jenekhe, S. A.; Bao, Z.; Xia, Y. Introducing Organic Nanowire Transistors. *Mater. Today* **2008**, *11* (4), 38–47. https://doi.org/10.1016/S1369-7021(08)70055-5.
- (30) Jo, S. B.; Lee, W. H.; Qiu, L.; Cho, K. Polymer Blends with Semiconducting Nanowires for Organic Electronics. *J. Mater. Chem.* **2012**, *22* (10), 4244–4260. https://doi.org/10.1039/C2JM16059E.
- (31) Kim, S.-M.; Kim, C.-H.; Kim, Y.; Kim, N.; Lee, W.-J.; Lee, E.-H.; Kim, D.; Park, S.; Lee, K.; Rivnay, J.; Yoon, M.-H. Influence of PEDOT:PSS Crystallinity and Composition on Electrochemical Transistor Performance and Long-Term Stability. *Nat. Commun.* **2018**, *9* (1), 3858. https://doi.org/10.1038/s41467-018-06084-6.
- (32) Kim, Y.; Noh, H.; Paulsen, B. D.; Kim, J.; Jo, I.-Y.; Ahn, H.; Rivnay, J.; Yoon, M.-H. Strain-Engineering Induced Anisotropic Crystallite Orientation and Maximized Carrier Mobility for High-

- Performance Microfiber-Based Organic Bioelectronic Devices. *Adv. Mater.* **2021**, *33* (10), e2007550. https://doi.org/10.1002/adma.202007550.
- (33) Wu, X.; Surendran, A.; Ko, J.; Filonik, O.; Herzig, E. M.; Müller-Buschbaum, P.; Leong, W. L. Ionic-Liquid Doping Enables High Transconductance, Fast Response Time, and High Ion Sensitivity in Organic Electrochemical Transistors. *Adv. Mater.* 2019, 31 (2), e1805544. https://doi.org/10.1002/adma.201805544.
- (34) Wan, A. M.-D.; Inal, S.; Williams, T.; Wang, K.; Leleux, P.; Estevez, L.; Giannelis, E. P.; Fischbach, C.; Malliaras, G. G.; Gourdon, D. 3D Conducting Polymer Platforms for Electrical Control of Protein Conformation and Cellular Functions. *J. Mater. Chem. B Mater. Biol. Med.* **2015**, *3* (25), 5040–5048. https://doi.org/10.1039/C5TB00390C.
- (35) Pitsalidis, C.; Ferro, M. P.; Iandolo, D.; Tzounis, L.; Inal, S.; Owens, R. M. Transistor in a Tube: A Route to Three-Dimensional Bioelectronics. *Sci Adv* **2018**, *4* (10), eaat4253. https://doi.org/10.1126/sciadv.aat4253.
- (36) Zhang, Y.; Li, J.; Li, R.; Sbircea, D.-T.; Giovannitti, A.; Xu, J.; Xu, H.; Zhou, G.; Bian, L.; McCulloch, I.; Zhao, N. Liquid-Solid Dual-Gate Organic Transistors with Tunable Threshold Voltage for Cell Sensing. ACS Appl. Mater. Interfaces 2017, 9 (44), 38687–38694. https://doi.org/10.1021/acsami.7b09384.
- (37) Du, W.; Ohayon, D.; Combe, C.; Mottier, L.; Maria, I. P.; Ashraf, R. S.; Fiumelli, H.; Inal, S.; McCulloch, I. Improving the Compatibility of Diketopyrrolopyrrole Semiconducting Polymers for Biological Interfacing by Lysine Attachment. *Chem. Mater.* 2018, 30 (17), 6164–6172. https://doi.org/10.1021/acs.chemmater.8b02804.
- (38) Xu, H.; Jiang, Y.; Li, J.; Ong, B. S.; Shuai, Z.; Xu, J.; Zhao, N. Spectroscopic Study of Electron and Hole Polarons in a High-Mobility Donor–Acceptor Conjugated Copolymer. *J. Phys. Chem. C* **2013**, *117* (13), 6835–6841. https://doi.org/10.1021/jp4003388.

- (39) Li, J.; Zhao, Y.; Tan, H. S.; Guo, Y.; Di, C.-A.; Yu, G.; Liu, Y.; Lin, M.; Lim, S. H.; Zhou, Y.; Su, H.; Ong, B. S. A Stable Solution-Processed Polymer Semiconductor with Record High-Mobility for Printed Transistors. Sci. Rep. 2012, 2, 754. https://doi.org/10.1038/srep00754.
- (40) Nielsen, C. B.; Turbiez, M.; McCulloch, I. Recent Advances in the Development of Semiconducting DPP-Containing Polymers for Transistor Applications. *Adv. Mater.* 2013, 25 (13), 1859–1880. https://doi.org/10.1002/adma.201201795.
- (41) Lei, Y.; Deng, P.; Li, J.; Lin, M.; Zhu, F.; Ng, T.-W.; Lee, C.-S.; Ong, B. S. Solution-Processed Donor-Acceptor Polymer Nanowire Network Semiconductors For High-Performance Field-Effect Transistors. *Sci. Rep.* **2016**, *6*, 24476. https://doi.org/10.1038/srep24476.
- (42) Um, H. A.; Lee, D. H.; Heo, D. U.; Yang, D. S.; Shin, J.; Baik, H.; Cho, M. J.; Choi, D. H. High Aspect Ratio Conjugated Polymer Nanowires for High Performance Field-Effect Transistors and Phototransistors. *ACS Nano* **2015**, *9* (5), 5264–5274. https://doi.org/10.1021/acsnano.5b01982.
- (43) Yang, S.-F.; Liu, Z.-T.; Cai, Z.-X.; Dyson, M. J.; Stingelin, N.; Chen, W.; Ju, H.-J.; Zhang, G.-X.; Zhang, D.-Q. Diketopyrrole-Based Conjugated Polymer Entailing Triethylene Glycols as Side Chains with High Thin-Film Charge Mobility without Post-Treatments. *Adv. Sci.* **2017**, *4* (8), 1700048. https://doi.org/10.1002/advs.201700048.
- (44) Moser, M.; Savva, A.; Thorley, K.; Paulsen, B. D.; Hidalgo, T. C.; Ohayon, D.; Chen, H.; Giovannitti, A.; Marks, A.; Gasparini, N.; Wadsworth, A.; Rivnay, J.; Inal, S.; McCulloch, I. Polaron Delocalization in Donor–Acceptor Polymers and Its Impact on Organic Electrochemical Transistor Performance. *Angew. Chem. Weinheim Bergstr. Ger.* 2021, 133 (14), 7856–7864. https://doi.org/10.1002/ange.202014078.
- (45) Krauss, G.; Meichsner, F.; Hochgesang, A.; Mohanraj, J.; Salehi, S.; Schmode, P.; Thelakkat, M. Polydiketopyrrolopyrroles Carrying Ethylene Glycol Substituents as Efficient Mixed Ion-electron Conductors for Biocompatible Organic Electrochemical Transistors. *Adv. Funct. Mater.* 2021, 2010048. https://doi.org/10.1002/adfm.202010048.

- (46) Pappa, A.-M.; Parlak, O.; Scheiblin, G.; Mailley, P.; Salleo, A.; Owens, R. M. Organic Electronics for Point-of-Care Metabolite Monitoring. *Trends Biotechnol.* 2017. https://doi.org/10.1016/j.tibtech.2017.10.022.
- (47) Rivnay, J.; Leleux, P.; Ferro, M.; Sessolo, M.; Williamson, A.; Koutsouras, D. A.; Khodagholy, D.; Ramuz, M.; Strakosas, X.; Owens, R. M.; Benar, C.; Badier, J.-M.; Bernard, C.; Malliaras, G. G. High-Performance Transistors for Bioelectronics through Tuning of Channel Thickness. *Sci Adv* 2015, *I* (4), e1400251. https://doi.org/10.1126/sciadv.1400251.
- (48) Kaphle, V.; Paudel, P. R.; Dahal, D.; Radha Krishnan, R. K.; Lüssem, B. Finding the Equilibrium of Organic Electrochemical Transistors. *Nat. Commun.* 2020, 11 (1), 2515. https://doi.org/10.1038/s41467-020-16252-2.
- (49) Urquhart, S. G.; Martinson, M.; Eger, S.; Murcia, V.; Ade, H.; Collins, B. A. Connecting Molecular Conformation to Aggregation in P3HT Using Near Edge X-Ray Absorption Fine Structure Spectroscopy. *J. Phys. Chem. C* 2017, *121* (39), 21720–21728. https://doi.org/10.1021/acs.jpcc.7b07143.
- (50) Carli, S.; Di Lauro, M.; Bianchi, M.; Murgia, M.; De Salvo, A.; Prato, M.; Fadiga, L.; Biscarini, F. Water-Based PEDOT:Nafion Dispersion for Organic Bioelectronics. ACS Appl. Mater. Interfaces 2020, 12 (26), 29807–29817. https://doi.org/10.1021/acsami.0c06538.
- (51) Brown, P. J.; Thomas, D. S.; Köhler, A.; Wilson, J. S.; Kim, J.-S.; Ramsdale, C. M.; Sirringhaus, H.; Friend, R. H. Effect of Interchain Interactions on the Absorption and Emission of Poly(3-Hexylthiophene). *Phys. Rev. B Condens. Matter* 2003, 67 (6), 064203. https://doi.org/10.1103/PhysRevB.67.064203.
- (52) Zhang, Y.; Han, G.; Qin, M.; Shen, Y.; Lu, X.; Yi, Y.; Zhao, N. Spectroscopic Study of Charge Transport at Organic Solid–Water Interface. *Chem. Mater.* 2018, 30 (15), 5422–5428. https://doi.org/10.1021/acs.chemmater.8b02260.

- (53) Shiri, P.; Dacanay, E. J. S.; Hagen, B.; Kaake, L. G. Dynamic Charging Mechanism of Organic Electrochemical Devices Revealed with In Situ Infrared Spectroscopy. *J. Phys. Chem. C* 2019, *123* (32), 19395–19401. https://doi.org/10.1021/acs.jpcc.9b05739.
- (54) Shiri, P.; Dacanay, E. J. S.; Hagen, B.; Kaake, L. G. Vogel–Tammann–Fulcher Model for Charging Dynamics in an Organic Electrochemical Transistor. *J. Mater. Chem.* 2019, 7 (41), 12935–12941. https://doi.org/10.1039/C9TC02563D.
- (55) Bischak, C. G.; Flagg, L. Q.; Yan, K.; Rehman, T.; Davies, D. W.; Quezada, R. J.; Onorato, J. W.; Luscombe, C. K.; Diao, Y.; Li, C.-Z.; Ginger, D. S. A Reversible Structural Phase Transition by Electrochemically-Driven Ion Injection into a Conjugated Polymer. *J. Am. Chem. Soc.* 2020, 142 (16), 7434–7442. https://doi.org/10.1021/jacs.9b12769.